Cui et al. *Zool. Res.* 2026, 47(3): 621−634
https://doi.org/10.24272/j.issn.2095-8137.2025.286
https://cstr.cn/32248.14.zr.2025.286

ZR | Zoological Research

Article Open Access

Integrated spatial transcriptomic and metabolic profiling identifies molecular networks associated with cognitive performance in the porcine prefrontal cortex

Sheng-Di Cui[1,2,#], Dong Chen[1,2,#], Zhen-Jian Zhao[1,2], Qi Shen[1,2], Yang Yu[1,2], Jun-Ge Wang[1,2], Zi-Yang Chen[1,2], Shi-Xin Yu[1,2], Jia-Miao Chen[1,2], Ping-Xian Wu[3,4], Zong-Yi Guo[3,4], Jin-Yong Wang[3,4], Xue-Wei Li[1,2], Guo-Qing Tang[1,2,*]

[1] *State Key Laboratory of Swine and Poultry Breeding Industry*, *College of Animal Science and Technology*, *Sichuan Agricultural University*, *Chengdu*, *Sichuan* 611130, *China*

[2] *Farm Animal Genetic Resources Exploration and Innovation Key Laboratory of Sichuan Province*, *College of Animal Science and Technology*, *Sichuan Agricultural University*, *Chengdu*, *Sichuan* 611130, *China*

[3] *Chongqing Academy of Animal Sciences*, *Chongqing* 402460, *China*

[4] *National Center of Technology Innovation for Pigs*, *Chongqing* 402460, *China*

ABSTRACT

Pigs possess advanced cognitive capabilities and provide a valuable large-animal model for studying human cognition and neurological disorders. To elucidate the molecular architecture underlying cognitive function, spatial transcriptomics and metabolomics were integrated to generate a high-resolution, multidimensional map of the porcine prefrontal cortex. This framework enabled precise localization of cognition-associated molecular programs within structurally complex neural tissue. Focusing on cortical layers III–V, the spatial distribution of transcripts and metabolites was systematically resolved, identifying *CHGB* as a cognition-linked gene associated with synaptic depolarization, cognitive performance, and neuropeptide secretion. Differential *CHGB* expression across cognitive groups was further validated through immunohistochemical analysis and Y-maze behavioral testing in stratified mouse models. Integrated gene-metabolite network reconstruction further implicated cortical aerobic glycolysis in cognitive regulation and revealed a layered molecular architecture that connected transcriptional activity, metabolic state, and neurochemical signaling. These findings provide the first spatially resolved multi-omics framework for a large gyrencephalic brain and establish a novel paradigm for advancing research in cognition-related mechanisms and neurodegenerative disease pathways.

Keywords: Spatial transcriptomics; Spatial metabolomics; Cognitive ability; Pigs

INTRODUCTION

Pigs have played a central role in livestock domestication as a vital source of meat and other agricultural products. Beyond agricultural importance, the porcine brain shows neurodevelopmental and neuroanatomical features that closely resemble those of the human brain (Ryan et al., 2018), including shared aspects of behavior and cortical lamination (Dai et al., 2018; Sorby-Adams et al., 2018; Vink, 2018). These characteristics support the use of pigs as a powerful large-animal model for investigating cognitive function and neurological disease, complementing non-human primate systems (Qiu & Li, 2017; Silverman et al., 2022). Unlike rodents, which have lissencephalic brains and abbreviated postnatal development, pigs provide greater physiological (Howard et al., 2018) and anatomical relevance for studying higher-order cognitive processes with greater similarity to human cognition (Swindle et al., 2012).

As a gyrencephalic species with complex cognitive capacities, the pig provides an important system for defining spatial molecular programs that contribute to individual variation in cognitive performance. Such knowledge could strengthen translational research on human neurocognitive health. Studies of porcine cognition not only contribute to improved animal welfare and agricultural management but also offer a valuable platform for biomedical research (Netzley & Pelled, 2023), including the modeling of human cognitive processes (Kornum & Knudsen, 2011) and neurological pathologies (Qiu et al., 2024; Todea et al., 2020).

Despite the translational value of porcine models, most omics studies of the porcine brain have lacked sufficient spatial resolution (Fang et al., 2012; Lin et al., 2000; Zhang

Received: 15 October 2025; Accepted: 10 November 2025; Online: 11 November 2025

Foundation items: This work was supported by the Sichuan Provincial Science and Technology Department Project (2021ZDZX0008, 2020YFN0024, 2021YFYZ0030) and National Pig Technology Innovation Centre Pilot Science and Technology Project (NCTIP-XD/B01)

[#]Authors contributed equally to this work

*Corresponding author, E-mail: tyq003@163.com

et al., 2013; Zhu et al., 2021), limiting mechanistic interpretation at the level of cortical layers. Recent advances in spatial multi-omics have enabled high-resolution molecular profiling within intact tissue architecture (Baysoy et al., 2023; Vandereyken et al., 2023), creating new opportunities to resolve the spatial underpinnings of cognition. These approaches overcome key limitations of tissue homogenization by preserving anatomical context, which is essential for analysis of the laminated cortex, where discrete layers mediate specialized neural functions.

In this study, spatial transcriptomics and metabolomics were combined to generate a layer-resolved molecular atlas of the porcine prefrontal cortex. Key findings were further evaluated in mouse models to assess cross-species conservation and strengthen translational relevance to human neurocognitive disorders, including Alzheimer's disease and schizophrenia. This work provides the first integrated spatial multi-omics resource for the porcine prefrontal cortex and establishes the pig as a critical bridging model for cognitive and translational neuroscience.

MATERIALS AND METHODS

Animal selection and cognitive testing

Cognitive performance was assessed using a free-foraging arena paradigm adapted from established exploratory choice tasks (Mendl et al., 1997) and food-concealment protocols (Friess et al., 2007). Six identical boxes were strategically arranged in a dedicated testing arena, with one box containing a food reward and the remaining five boxes left empty. During habituation, all boxes were inverted to expose the interior compartment and allow direct visual inspection by the piglets. Before each session, the arena and outer surfaces of all boxes were cleaned with Waco disinfectant solution to minimize olfactory cues.

For each habituation trial, two piglets were randomly selected and gently transferred to the testing arena. Animals were allowed to freely explore the arena for 10 min to reduce novelty-induced stress and become familiar with the spatial layout. Following this acclimation period, all boxes were returned to the upright position, with openings facing upward, thereby preventing direct visual inspection of the contents.

Each piglet was then allowed 3 min to explore the boxes and select a target. If the baited box was not located and investigated within this period, the target box was manually tipped over to expose the food reward, after which an additional 3 min of exploration was permitted. This procedure reinforced the association between the experimental context and food reward while promoting environmental familiarity.

After habituation was completed, all boxes were restored to the upright position, and a single baited box was used in each trial. Pairs of piglets were randomly selected without replacement and introduced into the arena for testing. Each piglet completed eight consecutive trials, each requiring exploration of all six boxes to identify the baited box.

All testing sessions were recorded using video equipment. Two behavioral parameters were quantified: time spent exploring the baited box (TEF) and time spent exploring the empty boxes (TEE). These measures were used to calculate the recognition index (RI) according to Equation (1), providing a quantitative index of exploratory performance and enabling classification of piglets with high or low cognitive performance.

$$RI = \frac{TEF}{TEF + TEE} \times 100\% \quad (1)$$

In addition to exploration time, the ability to identify the first explored box as the last baited box (FELF) was recorded to evaluate memory retention and use of prior task experience. The time required to find the food box (FTF), defined as the interval from trial initiation to successful location of the baited box, was also measured. This parameter provided a direct index of foraging efficiency and supported evaluation of working memory capacity and overall cognitive performance.

The foraging-based cognitive battery was adapted from validated paradigms used to assess exploratory motivation, working memory, and behavioral flexibility in pigs, processes that depend in part on prefrontal cortex function.

Piglets were stratified according to cognitive test performance. Animals were ranked by RI score, and the three highest-ranking and three lowest-ranking piglets were assigned to the high cognitive ability (HC) and low cognitive ability (LC) groups, respectively. The control group (CO) included two randomly selected piglets from the same pen that had not undergone cognitive testing, allowing assessment of potential effects associated with the testing procedure itself. In downstream molecular analyses, HC and LC groups were used as the primary comparison to identify cognition-associated molecular signatures, with the CO group serving as a secondary reference.

A simple maze was constructed with baffles in the experimental pen to further assess spatial navigation. HC and LC piglets were tested individually after placement in the innermost maze compartment. All trials were video recorded for behavioral analysis. Four parameters were quantified: time to escape from the maze (TEM), time spent moving in the maze (TMM), total time spent in the maze (TSM), and number of wrong turns (NW). These metrics provided objective behavioral measures for comparing cognitive performance between groups. The test was based on innate escape behavior and spatial navigation capacity in pigs, which have been shown to reflect working memory and cognitive flexibility (Kinder et al., 2019; Singh et al., 2019).

Sample processing

Healthy 6-week-old castrated male piglets (Landrace×Large White F1 cross) were used as experimental animals. Pigs were selected as a translational model because their gyrencephalic brain architecture and complex cognitive capacity provide closer neuroanatomical and functional relevance to humans than rodent models. Initial screening excluded animals with abnormal health status or delayed developmental progression. Twelve piglets were then randomly selected from the qualified population to preserve randomization and population representativeness and were used for cognitive testing and subsequent allocation to the HC, LC, and CO groups.

All piglets were maintained under identical housing conditions with controlled environmental parameters. Animals had *ad libitum* access to standardized feed and were housed at 24±1°C, 60%±5% relative humidity, and a 12:12 h light-dark cycle (lights on at 0800h) to minimize environmental confounding. The study protocol was approved by the Institutional Animal Care and Use Committee of Sichuan Agricultural University (Approval No. 20230369).

Following euthanasia, porcine brains were immediately harvested via craniotomy and flash-frozen in liquid nitrogen. Rapid cryopreservation was used to preserve cellular

architecture and biomolecular integrity, thereby ensuring sample quality for subsequent spatial transcriptomic and metabolomic analyses.

10x Genomics Visium spatial transcriptomics sequencing and data processing

Spatial transcriptomics analysis was performed on porcine prefrontal cortex samples described above. Frozen tissue samples were sectioned at 10 μm using a cryostat microtome under optimized temperature conditions to preserve tissue integrity and section uniformity. Sections were air-dried at room temperature, stained with hematoxylin and eosin (H&E), dehydrated through a graded ethanol series (70%, 85%, 95%, and 100%), cleared in xylene, and mounted for imaging. Sections were then fixed in 4% paraformaldehyde (PFA) for 30 min at 4°C, permeabilized with 0.1% Triton X-100 for 12 min, and blocked in prehybridization solution for 30 min. Processed sections were placed onto 10x Genomics Visium spatial gene expression slides containing RNA capture probes, with controlled pressure applied to ensure optimal tissue-probe contact during overnight incubation at 37°C. Following RNA capture, first-strand cDNA was synthesized by reverse transcription, and spatial transcriptomics libraries were constructed according to the 10x Genomics Visium protocol (CG000239 Rev D), incorporating unique molecular identifiers (UMIs) and spatial barcodes. Library quality was evaluated by Qubit fluorometric quantification, Bioanalyzer-based fragment profiling, and barcode sequence verification. Libraries that satisfied predefined quality thresholds (Q30>85%, fragment size 300–500 bp) were pooled and sequenced on an Illumina NovaSeq platform to generate raw FASTQ files for subsequent spatial analysis.

Raw sequencing data were processed through a spatial transcriptomics analysis workflow that integrated read-level quality control, genome alignment, spatial barcode assignment, normalization, clustering, cortical layer annotation, differential expression analysis, and functional enrichment. Raw FASTQ files were first filtered using fastp (v.0.23.2) (Chen, 2023; Chen et al., 2018), including adapter trimming, quality filtering at a Q20 threshold, and removal of low-quality reads shorter than 50 bp. Clean reads were aligned to the *Sus scrofa* reference genome (Sscrofa11.1) using Space Ranger (v.2.1.1) (Satija et al., 2015) with default parameters. This step assigned reads to genomic features while retaining spatial barcode information and generated gene expression matrices that incorporated transcriptional profiles and spatial coordinates, enabling subsequent quantitative analysis of location-specific gene expression patterns.

Data preprocessing and quality control were performed using Seurat (v.4.3.3) (Hao et al., 2021). Spot-level quality metrics are shown in Supplementary Figure S1. Data were normalized using SCTransform (v.0.3.5) to reduce technical artifacts while preserving biological signals. For integrated analysis, multiple samples were merged into a single Seurat object, followed by repeated SCTransform normalization to maintain cross-sample consistency. Principal component analysis (PCA) was then performed using RunPCA, with 50 principal components retained to balance information capture and computational efficiency. Batch effects were corrected using RunHarmony, with sample origin and slide identity specified as grouping variables (group.by.vars=sample) to account for experimental and technical variation.

After preliminary UMAP-based clustering and annotation of cortical layers and white matter regions based on established markers and spatial position, spots annotated as white matter regions were removed. Subsequent analyses therefore focused on cortical regions enriched for neuronal populations, improving the biological relevance of spatial transcriptomic investigations.

Following data integration and filtering, nonlinear dimensionality reduction was performed using the RunUMAP function (n_neighbors=30, min_dist=0.3) with principal components 1–30 as input features. Neighbor relationships among spots were established through k-nearest neighbor graph construction using FindNeighbors (k.param=20). Clusters were identified using FindClusters at a resolution of 0.5 with Louvain community detection. Clustering results were visualized using both UMAP embeddings and spatial coordinate projections, enabling simultaneous examination of transcriptional similarity (UMAP) and anatomical organization (spatial mapping). Six cerebral cortical layers were annotated based on established cortical laminar markers and spatial localization.

Differential expression analysis was conducted after preprocessing of the raw expression matrix using the Seurat normalization workflow, including NormalizeData with log normalization and a scale factor of 10 000, FindVariableFeatures to identify the top 2 000 highly variable genes, and ScaleData to center and scale gene expression values. Cluster marker genes were identified using the Wilcoxon rank-sum test implemented in FindAllMarkers, ranked by $\log_2$ fold change ($\log_2$FC), and the top 10 markers for each cluster were visualized in a heatmap. Intergroup differentially expressed genes (DEGs) were identified using FindMarkers with the Wilcoxon test and stringent thresholds of adjusted $P<0.05$ and $|\log_2 FC|>0.25$. Kyoto Encyclopedia of Genes and Genomes (KEGG) enrichment analysis was performed for significant DEGs using clusterProfiler (Yu et al., 2012) (*P*-adjustment="BH", organism="ssc") to identify enriched biological pathways and functional programs associated with cortical layer-specific functions.

Airflow-assisted desorption electrospray ionization mass spectrometry imaging (AFADESI-MSI) and spatial metabolomic data analysis

Spatial metabolomics imaging was performed in both positive and negative ionization modes to expand metabolite coverage across chemically diverse molecular classes. Positive ionization mode preferentially ionizes basic compounds such as amino acids and lipids, while negative ionization mode enhances the detection of acidic metabolites, including organic acids, sugars, and phosphorylated compounds. This dual-mode approach increased metabolome coverage, enabling the detection of a wider range of biochemical pathways potentially relevant to cognitive function.

Data were acquired using a Waters Synapt XS high-resolution mass spectrometer operated in both ionization modes. Tissue sections were analyzed under optimized atmospheric-pressure ionization conditions using an acetonitrile/water (80:20, v/v) mobile phase delivered at 2 μL/min. Ionization parameters included a 3 mm tissue-to-sprayer distance, 5 mm sprayer-to-transfer tube distance, and 60° spray angle, with the ion source temperature maintained at 150°C. The desolvation gas pressure was set to 0.6 MPa for efficient ionization. Imaging was performed with a continuous scanning speed of 200 μm/s along the x-axis and 100 μm steps along the y-axis. Spectra were acquired across

an m/z range of 70–1 200 Da at a mass resolution of 20 000 full width at half maximum (FWHM). The resulting data provided a pixel size of 50×50 μm, enabling high-resolution spatial mapping of metabolites across porcine prefrontal cortex tissue sections.

Spatial metabolomic data were processed through a standardized workflow. Raw files were converted to .imzML format using imzMLConverter (Race et al., 2012), followed by preprocessing in Cardinal (v.3.10.0) (Bemis et al., 2023), including background subtraction, peak alignment, and feature filtering. Metabolites were annotated against the SmetDB database using pySM based on m/z values, fragment ions, and retention time. Spatial clustering, heatmaps of top metabolites, and dimensionality reduction using t-SNE and UMAP were applied to visualize metabolic organization across tissue regions. Differentially abundant metabolites between cognitive groups were identified using Wilcoxon tests, and KEGG enrichment analysis was performed to identify significantly altered metabolic pathways.

This spatial metabolomic workflow provided functional metabolic information that complemented the spatial transcriptomic data and supported construction of spatially resolved gene-metabolite interaction networks.

Weighted gene co-expression network analysis (WGCNA)

Spatial transcriptomic and metabolomic datasets provide complementary molecular information, with the former capturing layer-specific gene expression patterns and the latter revealing the spatial distribution of metabolite features. Integration of these data enabled construction of gene-metabolite co-expression networks within the spatial architecture of cortical layers, thereby linking transcriptional organization to metabolic state in a tissue-contextualized framework.

Weighted co-expression networks were constructed separately for metabolomic and transcriptomic datasets using standard WGCNA procedures, including data standardization, correlation estimation, soft-thresholded adjacency matrix construction, module identification, and module eigengene calculation. For spatial metabolomic data, feature matrices were converted into Seurat objects and standardized before network analysis. For both molecular layers, the pickSoftThreshold function in hdWGCNA (Morabito et al., 2023) was used to determine the optimal soft-thresholding power (β), with selection guided by a scale-free topology fit index (R^2) ≥0.8 while retaining adequate mean connectivity. This criterion supported construction of networks with biologically interpretable scale-free topology.

Weighted co-expression networks were then generated using blockwiseModules to identify modules of highly correlated metabolites or genes. For the metabolite network, the minimum module size was set to 50, and the module merge cut height was set to 0.2. The same analytical framework was applied to gene network construction. Following module detection, the module eigengene (ME) was calculated for each module. The ME, defined as the first principal component of a module, represented the dominant abundance or expression pattern of all features assigned to that module.

Modules associated with cognitive performance were identified by calculating Pearson correlation coefficients (r) and corresponding P values between each ME and cognitive traits, including RI, TEF, and NW. To integrate spatial transcriptomic and metabolomic layers, Pearson correlations were further calculated between gene module MEs and metabolite module MEs. This ME-ME correlation analysis identified significant associations between coordinated gene expression programs and metabolic states. Gene-metabolite module pairs with $|r|>0.3$ and $P<0.001$ were considered significantly associated and were used to construct the integrated network.

Within significant modules, hub genes were identified according to module membership (kME), with |kME|>0.6 indicating highly connected intramodular features. These hub genes were prioritized for biological interpretation as they are likely to play core regulatory roles in the functional outcomes of their respective modules.

Immunohistochemistry

Immunohistochemical (IHC) staining was performed to validate CHGB protein expression identified by spatial transcriptomic analysis and provide orthogonal confirmation of the omics findings at the protein level. Prefrontal cortex sections from the HC, LC, and CO groups were included for comparative analysis.

Frozen sections were equilibrated to room temperature, immersed in purified water for 3–5 min, and subjected to antigen retrieval in citrate buffer (pH 6.0) by microwave heating until boiling, followed by heat maintenance and natural cooling. Sections were then washed three times with phosphate-buffered saline (PBS, pH 7.4) for 5 min per wash. Endogenous peroxidase activity was quenched by incubation with 3% hydrogen peroxide for 25 min at room temperature away from light, followed by three additional PBS washes (5 min each).

After excess buffer was removed, tissue areas were outlined with a hydrophobic histochemical pen and blocked with 3% bovine serum albumin (BSA) for 30 min. Blocking solution was removed, and sections were incubated overnight at 4°C with primary antibody against *CHGB* diluted in PBS. After three PBS washes (5 min each), horseradish peroxidase (HRP)-conjugated secondary antibody specific to the primary antibody species was added and incubated for 50 min at room temperature. Unbound secondary antibody was removed by three PBS washes (5 min each), and staining was developed with 3,3'-diaminobenzidine (DAB). The chromogenic reaction was terminated by rinsing sections with tap water.

Cell nuclei were counterstained with hematoxylin for 3 min, differentiated to enhance nuclear contrast, and blued. Sections were then dehydrated through a graded ethanol series (75%, 85%, 100% I, and 100% II) for 5 min per step, cleared in xylene I for 5 min, dried, and sealed with neutral gum. Stained sections were examined by light microscopy, and digital images were collected for subsequent quantitative analysis of staining intensity using ImageJ. CHGB protein abundance was compared between the HC and LC groups to assess whether the transcriptional differences detected by spatial transcriptomics were reflected at the protein level.

Cognitive phenotyping and molecular validation in mice

A parallel mouse cohort was used to evaluate cross-species conservation of cognition-associated candidate genes identified in the porcine model and to determine whether expression patterns were associated with cognitive performance. This validation strategy also established a tractable experimental basis for future functional studies.

Twenty-five male C57BL/6J mice (6 weeks old) were selected and acclimatized for 2 weeks before behavioral testing. Working memory and exploratory behavior were

assessed using the Y-maze test. One day before formal testing, mice underwent a 5 min habituation session in the maze. During testing, each mouse was placed in one arm and allowed to explore freely for 8 min. Spontaneous alternation rate, calculated from the first 30 entries, was used to quantify short-term working memory. After 24 h, spatial novelty preference was assessed during a 5 min session by recording entries into and time spent in the previously blocked arm. Mice were ranked according to combined performance across spontaneous alternation and novelty preference measures, and the three highest- and three lowest-ranking animals were assigned to the HC and LC groups, respectively. Two additional naïve mice that did not undergo behavioral testing served as a CO baseline group.

For molecular validation, brain tissue was dissected from the screened mice, and total RNA was extracted using TRIzol reagent. Expression of candidate genes was measured by reverse transcription quantitative polymerase chain reaction (RT-qPCR), with three biological replicates included for each reaction to ensure data reliability. Relative expression was calculated using the $2^{-\Delta\Delta Ct}$ method. Ct values were first normalized to β-actin, which served as an internal reference gene with stable expression across groups, and fold changes in candidate gene expression were then calculated relative to the CO group. This analysis identified molecular differences between mice with high and low cognitive performance and provided cross-species support for candidate genes associated with cognitive function.

Single-cell RNA sequencing (RNA-seq) analysis of cell type-specific expression

Cell type-specific expression patterns of candidate genes were examined through secondary analysis of a publicly available single-cell RNA-seq atlas of the porcine prefrontal cortex (accession no.: CNP0000686) (Zhu et al., 2021). Raw sequencing data were processed using Cell Ranger (v.7.2.0) (Zheng et al., 2017).

Rigorous quality control retained cells with more than 200 detected genes and less than 5% mitochondrial gene content. Putative doublets were identified and removed using DoubletFinder (v.2.0.3) (McGinnis et al., 2019), with the expected doublet formation rate set to 0.075.

Quality-filtered data were normalized and scaled in Seurat. Log normalization was performed using NormalizeData with a scale factor of 10 000, and the 2 000 most variable genes were selected using FindVariableFeatures. Expression levels were then centered and standardized using ScaleData. PCA was performed on the highly variable gene set, and the first 20 principal components were retained for graph-based clustering and UMAP visualization.

Cluster-enriched marker genes were identified using FindAllMarkers with thresholds of logfc.threshold=0.25 and min.pct=0.1. *P*-values were adjusted using the Bonferroni method, with adjusted $P<0.05$ considered significant. Cell identities were assigned by comparing cluster marker profiles with established neural cell type markers from published single-cell studies (Campbell et al., 2017; Lau et al., 2020; Moffitt et al., 2018; Poulin et al., 2020). This annotated single-cell map was used to localize candidate gene expression across neuronal and non-neuronal compartments of the porcine prefrontal cortex. Because the public single-cell dataset and the spatial transcriptomic dataset were generated independently, possible batch effects precluded direct quantitative integration. Accordingly, this analysis served as an orthogonal reference for qualitative assignment of candidate genes to specific cellular populations.

RESULTS

To systematically define the molecular basis underlying variation in porcine cognitive performance, behavioral phenotypes were first quantified, followed by layer-resolved spatial transcriptomic and metabolomic profiling of the prefrontal cortex and integrative reconstruction of gene-metabolite regulatory networks.

Cognitive performance assessment and group stratification in piglets

Piglets were stratified by cognitive ability using a foraging-based behavioral battery (Figure 1A) and a maze test (Figure 1B), which assessed behavioral domains linked to prefrontal cortex function, including exploratory drive, working memory, and behavioral flexibility. Based on their performance, piglets were assigned to HC and LC groups for downstream molecular profiling.

HC piglets spent significantly more time exploring the baited box (TEF; $P=0.0073$; Cohen's d=0.8497) and empty boxes (TEE; $P=0.0126$; Cohen's d=0.7751), indicating greater exploratory engagement during the foraging task. The HC group also showed a higher RI ($P=0.0047$; Cohen's d=0.9721), consistent with more accurate decision-making (Figure 1C–E). Furthermore, HC piglets exhibited a markedly shorter latency to locate the baited box (FTF; $P=0.0123$; Cohen's d=−0.7632), suggesting improved spatial recall efficiency (Figure 1F). Although the FELF metric did not differ significantly between groups, the overall behavioral profile indicated stronger foraging performance, exploratory engagement, and spatial memory in HC piglets than in LC piglets.

In the maze test, HC piglets showed longer TEM, TMM, and TSM values, consistent with more extensive exploration of the unfamiliar environment and a more assessment-oriented navigation strategy. HC piglets also showed a higher number of wrong turns, suggesting greater novelty-driven exploration and behavioral adaptability in unfamiliar contexts (Supplementary Figure S2 and Table S1). These reproducible behavioral differences provided a phenotypic framework for testing whether cognitive stratification was associated with distinct spatial gene expression profiles in the prefrontal cortex.

Spatial transcriptomics reveals layer-specific gene expression associated with cognitive variation in pigs

To determine whether behavioral variation in cognition was accompanied by spatially organized transcriptional differences, spatial transcriptomic profiling was performed across cortical layers I–VI of the porcine prefrontal cortex, a principal region for integrative processing, executive control, and cortical output.

Histological assessment by H&E staining confirmed well-preserved prefrontal cortical architecture with minimal white matter contamination. Spatial transcriptomic profiling using the 10x Genomics Visium platform generated data from eight samples, yielding a median of 9 632 UMIs and 3 259 genes per spot, with an average of 8 103 spots per sample (Figure 2A). Raw data were processed with Space Ranger and analyzed in Seurat.

Following integration, normalization, and UMAP-based clustering, 10 transcriptionally distinct clusters were identified

(Figure 2B; Supplementary Figure S3A). Six cortical layers and a white matter region were annotated according to spatial position and cluster structure, whereas unclassified clusters were excluded. A total of 7 154 spots were retained for downstream analyses (Supplementary Figure S3D–K). PCA confirmed that variation among samples was primarily driven by biological differences rather than technical effects, supporting the robustness of the spatial transcriptomic dataset (Supplementary Figure S3B, C).

Layer-specific transcriptional programs were then defined through enrichment analysis of highly expressed genes in each cortical layer (Figure 2C; Supplementary Table S2). Layer I showed significant enrichment of pathways associated with cell adhesion, extracellular matrix (ECM) organization, and adherens junctions, including focal adhesion and ECM-receptor interaction, consistent with a role in synaptic integration and signal modulation. Layer II was enriched mainly in oxidative phosphorylation and energy metabolism, reflecting elevated local metabolic demand. Layer III showed pronounced enrichment of dopaminergic, cholinergic, and glutamatergic synapse pathways, together with long-term potentiation and long-term depression, highlighting the involvement of this layer in neural plasticity and higher-order associative processing. Layer V was enriched in synaptic vesicle cycling, GABAergic synapses, and oxidative phosphorylation, consistent with the role of this layer in cortical output and inhibitory regulation under high energetic demand. Layer VI was associated with glutamatergic signaling and ion homeostasis pathways, supporting its contribution to thalamocortical communication (Figure 2D; Supplementary Table S3).

To identify transcriptional correlates of cognitive performance, gene expression was compared between HC and LC piglets within cortical layers (Figure 2E; Supplementary Table S4). In layer III, a key hub for associative processing, HC piglets exhibited increased expression of genes implicated in neurodegeneration-related pathways, including *PRNP*, *COX1*, and *ATP6*, as well as genes involved in oxidative phosphorylation, including *ND4*, *ND5*, and *COX3*. This pattern suggests enhanced mitochondrial activity together with potential engagement of neuroprotective mechanisms. These differences were accompanied by altered expression of synaptic signaling genes, including *CAMK2A*, *SYT2*, and *GRIA2*. Additional layer-specific signatures were observed across the cortex. Layer II showed increased expression of ribosomal genes, including *RPS28* and *RPL37*, and genes annotated to coronavirus disease-related pathways, while layer IV showed enrichment of genes involved in ion transport and endocrine signaling, including *ATP2B2* and *ATP1A2*. Together, these findings suggest that cognitive ability is associated with spatially distributed transcriptional reprogramming involving energy metabolism, neuroprotection, and synaptic communication (Figure 2F; Supplementary Table S5).

These layer-specific transcriptional differences indicate that HC piglets maintained stronger neuronal homeostasis and metabolic efficiency, particularly in cortical layers involved in integrative processing. Because synaptic activity imposes substantial energetic demands, spatial metabolomic profiling was next performed to determine whether these transcriptional signatures were accompanied by layer-specific metabolic alterations.

Spatial metabolomics reveals layer-specific metabolic signatures associated with cognitive performance in pigs

To determine whether cognitive stratification was accompanied by spatially organized metabolic variation in the prefrontal cortex, spatial metabolomic profiling was conducted on tissue sections adjacent to those used for transcriptomic analysis. AFADESI-MSI detected 447 metabolites in positive ion mode and 1 317 metabolites in negative ion mode, encompassing major biochemical classes, including amino acids, lipids, organic acids, and sugars. UMAP dimensionality

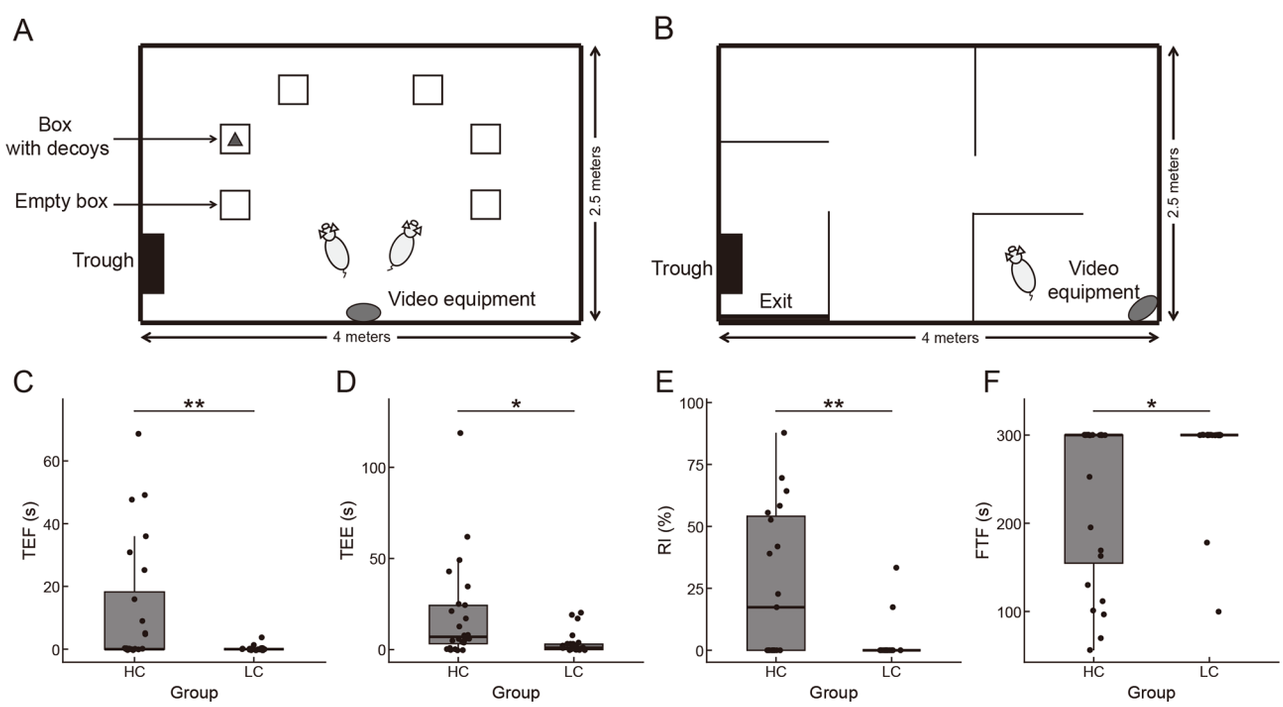

Figure 1 Experimental apparatus and behavioral performance in foraging-based and maze cognitive tests

A: Schematic representation of foraging-based test. B: Schematic representation of maze test. C–F: Box plots of foraging-based test results. *: $P<0.05$; **: $P<0.01$.

reduction and spatial clustering with the SSCC algorithm resolved 14 metabolically distinct regions in each ionization mode, with high spatial coherence across clusters (profile coefficients>0.7; Figure 2G).

Wilcoxon-based differential abundance analysis identified 155 metabolites in positive ion mode and 216 metabolites in negative ion mode that differed significantly between HC and LC piglets (Figure 2H; Supplementary Table S6). KEGG enrichment analysis showed that HC piglets had increased representation of pathways involved in branched-chain amino acid metabolism, arginine biosynthesis, pantothenate and CoA biosynthesis, and neuroactive sphingolipid metabolism, consistent with enhanced energy metabolism, synaptic signaling, and membrane stability (Figure 2I; Supplementary

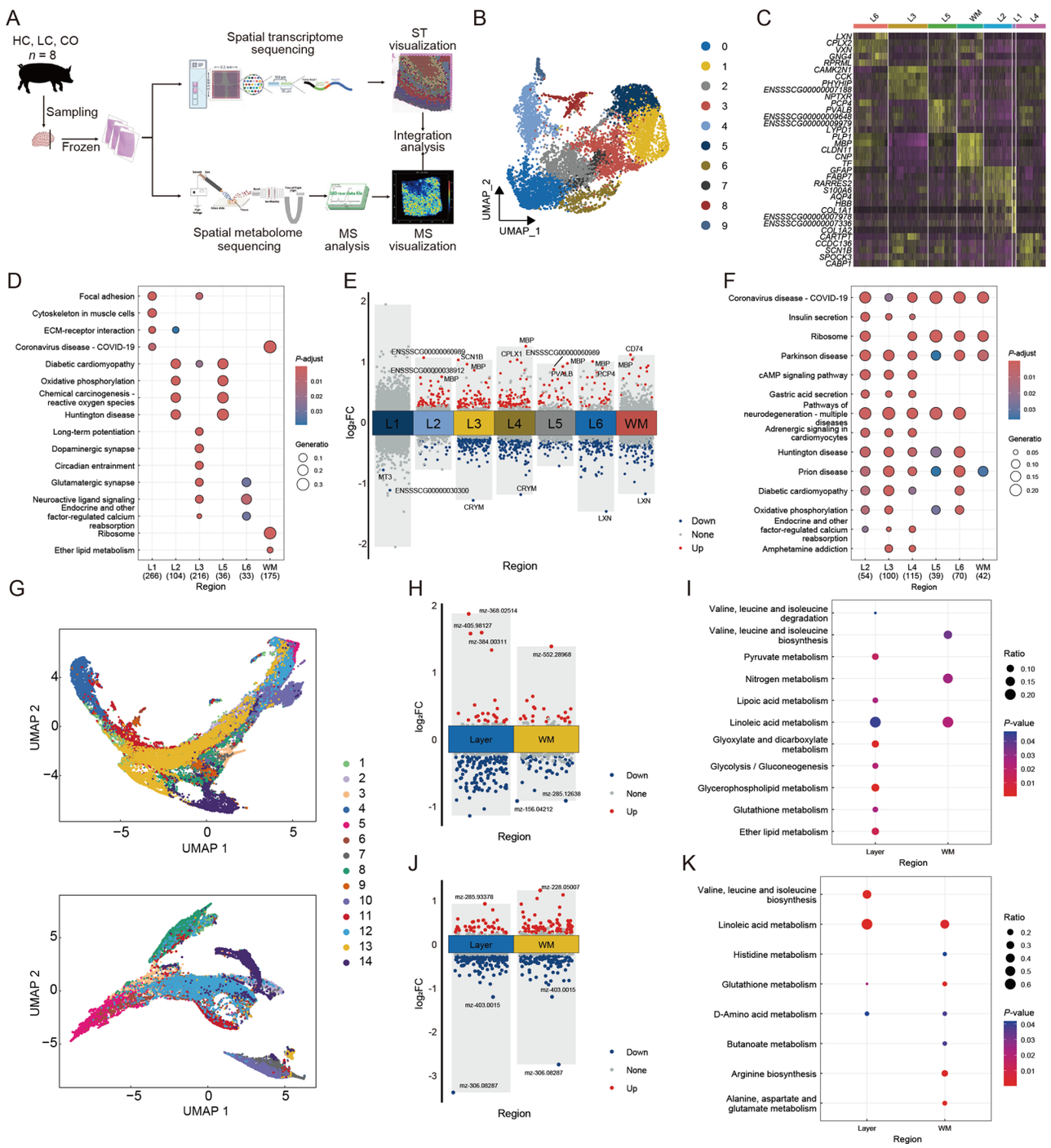

Figure 2 Spatial transcriptomic and metabolomic profiling of region-specific molecular signatures

A: Schematic overview of the spatial transcriptomic and metabolomic workflow. B: UMAP visualization of spatial transcriptomic profiles. C: Heatmap showing region-specific gene expression signatures. D: KEGG enrichment analysis of region-specific genes. E: Volcano plot showing differentially expressed genes between HC and LC groups. F: KEGG enrichment analysis of regional DEGs between HC and LC groups. G: UMAP visualization of spatial metabolomic profiles in positive ion mode (top) and negative ion mode (bottom). H: Regional volcano plots showing differential metabolite abundance between HC and LC groups in positive ion mode. I: Regional KEGG enrichment analysis of metabolites detected in positive ion mode. J: Regional volcano plots showing differential metabolite abundance between HC and LC groups in negative ion mode. K: Regional KEGG enrichment analysis of metabolites detected in negative ion mode.

Table S7).

Positive ion mode revealed prominent lipid-associated metabolic differences in HC piglets. Spatial transcriptomic profiles from corresponding cortical regions further indicated coordinated activation of lipid mediator synthesis and membrane structural programs. Up-regulated genes included *PTGDS*, which participates in prostaglandin metabolism and may support anti-inflammatory mediator production, as well as *PLP1* and *MBP*, which are essential for myelin organization and membrane integrity. Elevated expression of *FABP7*, a gene associated with fatty acid binding and neuroprotective signaling, further indicated enhanced lipid raft stability, myelin maintenance, and anti-inflammatory signaling. These convergent transcriptomic and metabolomic signatures suggest a lipid-centric adaptive mechanism that may contribute to improved cognitive function.

Negative ion mode highlighted pronounced metabolic differences related to amino acid turnover and energy metabolism in HC piglets. Increased expression of key genes involved in glutamate and aspartate metabolism, including *ATP1A2*, *SLC25A3*, and *SLC25A5*, suggested more efficient nitrogen handling and neurotransmitter cycling. Up-regulation of mitochondrial electron transport chain genes, including *COX1*, *COX3*, *ATP6*, *ND2*, *ND4*, and *ND5*, together with increased expression of the glycolytic enzyme *ENO1*, indicated elevated energetic capacity in specific cortical layers. Additionally, increased expression of genes related to glutathione metabolism (*GLRX* and *PRDX5*) and neuroactive peptide synthesis (*PENK* and *TAC1*) implied enhanced redox homeostasis and neuromodulatory capacity. Collectively, these metabolic signatures point to a shift toward sustained energy production and efficient neural signaling, supporting superior cognitive performance (Figure 2J).

Overall, HC piglets exhibited spatial metabolic features consistent with more efficient lipid utilization, mitochondrial energy production, and neuroprotective signaling. Importantly, many differentially abundant metabolites correlated with transcriptional changes in corresponding cortical layers, supporting coordinated gene-metabolite regulation as a molecular basis for cognitive variation (Figure 2K). To integrate these multimodal signatures, combined gene-metabolite modules were constructed and assessed for associations with cognitive traits.

Construction of integrated gene-metabolite co-expression networks reveals regulatory hubs associated with cognitive differences

To define systems-level mechanisms linking transcriptional and metabolic organization to cognitive performance, weighted gene co-expression networks were constructed from spatial transcriptomic profiles, and metabolite co-expression networks were constructed from spatial metabolomic profiles. These molecular layers were then integrated through module-module correlation analysis to identify coordinated gene-metabolite programs associated with cognitive variation.

Spatial metabolomic network analysis identified three metabolite modules in positive ion mode and five metabolite modules in negative ion mode (β=4 for both; Supplementary Figure S4). Associations between these metabolite modules and cognitive traits were then evaluated (Figure 3A, B). Spatial transcriptomic network analysis identified nine gene co-expression modules (β=4; Supplementary Figure S5A–D), each showing distinct laminar distributions across the prefrontal cortex. The blue, magenta, turquoise, pink, and brown modules were enriched in layer III; the yellow and black modules were enriched in layer I; the red module was enriched in layer IV; and the green module was enriched in layer VI (Supplementary Figure S5E). Comparison between cognitive groups showed increased expression of the red and turquoise modules in HC piglets (Supplementary Figure S5F), indicating potential roles in molecular programs associated with higher cognitive performance.

Functional annotation revealed strong biological concordance between the negative-ion yellow metabolite module and the turquoise gene module. These modules exhibited shared enrichment in pathways related to amino acid metabolism, particularly glutamate metabolism, as well as energy metabolism, including butanoate metabolism and oxidative phosphorylation, oxidative stress regulation through glutathione metabolism, and nucleotide metabolism. This convergence implicated coordinated regulation of neurotransmission, energy homeostasis, and cellular defense, consistent with synaptic and neurodegeneration-related functions represented in the turquoise gene module.

The negative-ion brown metabolite module, enriched for central carbon and redox pathways, including the tricarboxylic acid (TCA) cycle, pyruvate metabolism, and glutathione metabolism, showed close correspondence with the red gene module. Functional features of the red gene module were dominated by altered energy metabolism and oxidative stress programs. Together, these paired modules reflect core molecular processes implicated in metabolic dysfunction, oxidative injury, and disease-associated tissue remodeling, including pathways relevant to cancer, cardiovascular disease, and neurodegenerative disorders.

The negative-ion yellow metabolite module also aligned strongly with the magenta gene module, linking neurotransmitter metabolism (glutamate), antioxidant activity (glutathione), immunovascular regulation (arginine), and gut-brain axis signaling (butyrate) to transcriptional programs involved in nervous system regulation, neuroprotection, and multisystem adaptation to environmental challenges (Figure 3C, D; Supplementary Figure S5G, H; Supplementary Tables S8, S9).

Together, the integrated gene-metabolite modules defined a coordinated biological framework in which transcriptional programs related to neuroendocrine, immune, and cellular stress responses were coupled to metabolic features that function as signaling molecules, energy substrates, and protective mediators. This network architecture suggested that cognitive variation in piglets was associated with coordinated regulation of cortical energy metabolism, neurotransmitter cycling, redox balance, lipid signaling, and adaptive stress responses, with potential relevance to maladaptive neural states and neurodegenerative processes. The turquoise gene module and the associated amino acid and lipid metabolic modules were therefore prioritized as a candidate regulatory network linking metabolic state, synaptic function, and cognitive performance for downstream functional validation.

Key gene screening identifies layer-enriched candidates associated with cognitive performance

Candidate genes were prioritized for functional validation using three integrated criteria: enriched expression within defined cortical layers, significant differential expression between HC and LC piglets, and high intramodular connectivity within cognition-associated WGCNA modules, particularly the turquoise and red modules. This strategy

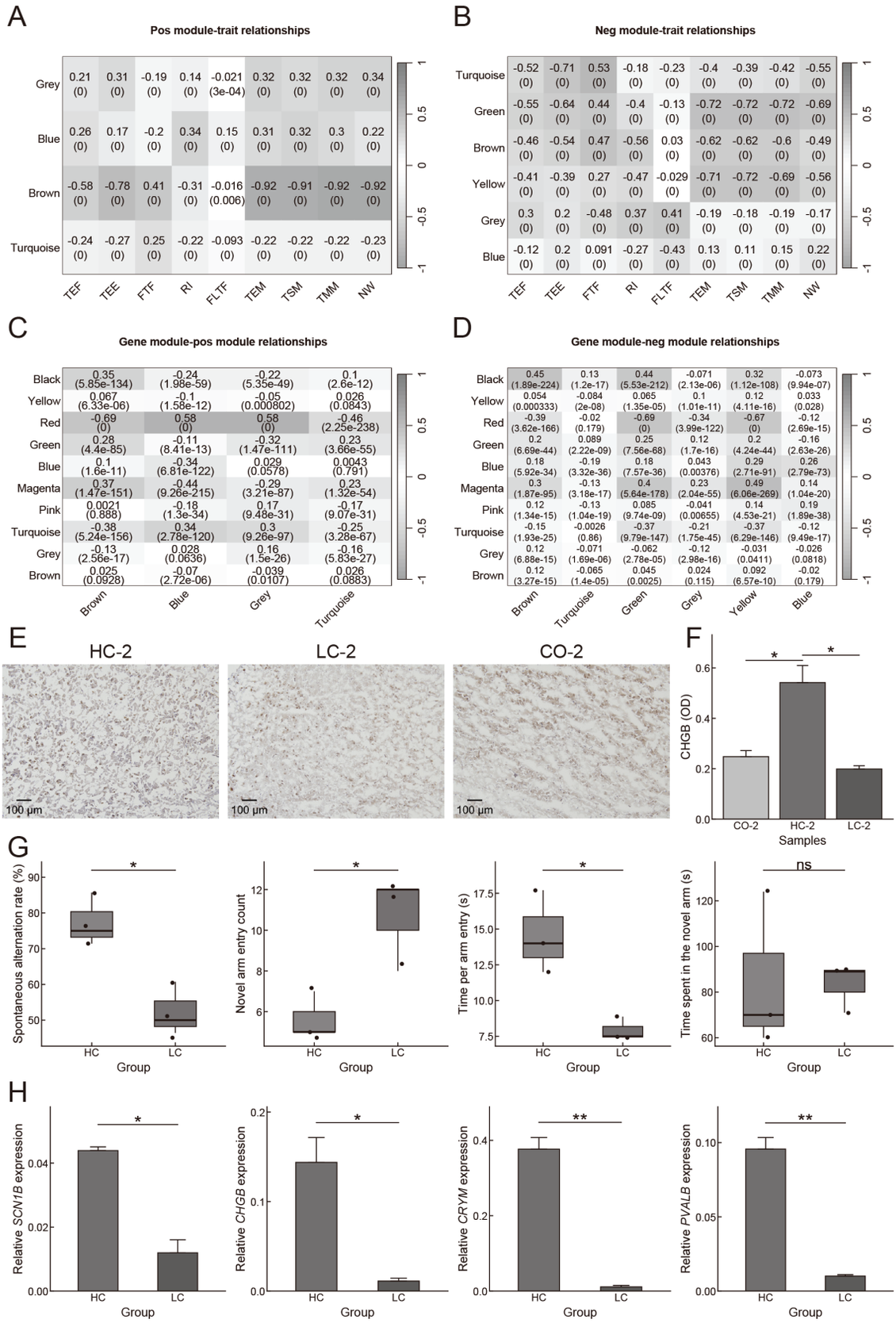

Figure 3 Multi-omics module correlation analysis links cognitive traits with gene-metabolite networks and experimental validation

A: Correlation heatmap showing associations between positive ion mode metabolite modules and cognitive traits. B: Correlation heatmap showing associations between negative ion mode metabolite modules and cognitive traits. C: Correlation heatmap showing associations between gene modules and positive ion mode metabolite modules. D: Correlation heatmap showing associations between gene modules and negative ion mode metabolite modules. E: Immunohistochemical staining of CHGB in prefrontal cortical tissue. F: Quantification of *CHGB* immunohistochemical staining intensity by optical density. G: Cognitive performance in HC and LC mice based on behavioral testing. H: RT-qPCR analysis of key gene expression in HC and LC mice. ns: $P>0.05$; *: $P<0.05$; **: $P<0.01$.

enabled selection of genes that were not only spatially localized and behaviorally associated but also centrally positioned within coordinated transcriptional programs.

Integrated analysis of differential expression and WGCNA identified several biologically relevant candidates with distinct laminar distributions. In layer III, a cortical layer strongly implicated in cognitive performance, multiple genes showed significant group-dependent expression and high module connectivity. *CHGB* and *NRGN*, both assigned to the turquoise module, are associated with neurosecretory processes and synaptic plasticity, respectively. *PVALB* and *SCN1B*, both in the red module, are associated with calcium signaling and neuronal excitability. Additionally, *CRYM*, assigned to the magenta module, was down-regulated in the HC group, suggesting a potential role in thyroid hormone metabolism and neural function. In layer VI, up-regulation of *MBP* in the green module suggested enhanced myelination, which may support efficient signal transmission. Conversely, down-regulation of *CAMK2N1* (blue module) in layer III suggested layer-specific modulation of calcium/calmodulin-dependent signaling pathways.

Together, these findings define a set of layer-specific and network-central candidate genes that may contribute to neural computation and cognitive performance. Therefore, these genes were subsequently validated through cross-species comparisons and experimental assays.

Immunohistochemistry reveals high CHGB protein abundance in HC piglets

Immunohistochemical staining was performed to determine whether transcriptional differences in CHGB, a high-priority candidate from the turquoise module, were reflected at the protein level in prefrontal cortical tissue from HC, LC, and CO piglets.

Quantitative optical density (OD) analysis revealed significantly higher CHGB protein expression in the HC group than in the LC and CO groups (Figure 3E, F). This finding is consistent with the spatial transcriptomic data and supports the correlation between elevated *CHGB* expression and enhanced cognitive performance.

These results suggest that *CHGB* may contribute to cognitive variation through mechanisms related to neuropeptide processing, regulated secretion, and synaptic modulation.

Y-maze testing identifies mice with divergent cognitive performance for cross-species validation

To assess conservation of cognition-associated molecular signatures identified in pigs, a similar cognitive stratification strategy was applied to C57BL/6J mice using the Y-maze test (Supplementary Figure S6A, B).

HC mice displayed a significantly higher spontaneous alternation rate than LC mice (P=0.0146), indicating superior working memory and cognitive flexibility. Although HC mice entered the novel arm less frequently (P=0.0452), they spent more time during each entry (P=0.0491), suggesting a more sustained and selective exploration pattern consistent with enhanced spatial encoding and memory retention (Figure 3G; Supplementary Table S10).

These behavioral differences established a mouse cohort with divergent cognitive performance, enabling cross-species molecular comparisons to evaluate whether cognition-associated prefrontal gene expression signatures identified in pigs are conserved in mice.

Gene expression analysis reveals conserved cognition-associated signatures in mice

To examine cross-species conservation of candidate genes identified in pigs, prefrontal cortex expression of these genes was quantified in HC and LC mice. Notably, *SCN1B*, *CRYM, CHGB*, and *PVALB* showed significantly higher expression in HC mice than in LC mice (Figure 3H; Supplementary Figure S6C–G and Table S11), consistent with the expression patterns observed in pigs and supporting conserved associations with cognitive performance.

In contrast, *NRGN* and *CAMK2N1* did not exhibit significant differences between HC and LC mice. *CAMK2N1* showed high expression during early neurodevelopment but did not vary significantly across adult cognitive-performance groups, suggesting a developmental role rather than a direct association with adult cognitive variation.

Together, the conserved up-regulation of *SCN1B*, *CRYM*, *CHGB*, and *PVALB* in high-performing individuals across species suggests that these genes may participate in an evolutionarily conserved network associated with cognitive ability. These cross-species results highlight promising candidates for further functional investigation using targeted perturbation approaches, including CRISPR-based models or human induced pluripotent stem cell-derived neuronal systems.

Single-cell transcriptomics reveals cell type-specific expression of key cognition-associated genes

After stringent quality control and doublet removal, single-cell transcriptomic analysis retained 7 439 high-quality cells from the porcine prefrontal cortex dataset. UMAP-based dimensionality reduction and unsupervised clustering resolved 17 transcriptionally distinct clusters, which were annotated into seven major cell types using cluster-enriched marker genes (Supplementary Figure S6H, I and Table S12).

Expression analysis of the cognition-associated candidates *CHGB, CRYM*, *PVALB*, and *SCN1B* revealed clear cellular specialization. *CHGB* and *CRYM* were preferentially expressed in excitatory glutamatergic neurons, whereas *PVALB* and *SCN1B* were predominantly enriched in inhibitory GABAergic neurons (Supplementary Figure S6J). These cell type-resolved patterns indicate that cognition-associated genes in the porcine prefrontal cortex show distinct enrichment across excitatory and inhibitory neuronal populations, providing cellular context for their potential roles in cognitive regulation.

DISCUSSION

Spatial molecular architecture and cellular basis of cognitive function

Laminar organization is a defining feature of cerebral cortical specialization (Balaram & Kaas, 2014; Bastos et al., 2018), with layer III playing a central role in associative processing and higher cognitive operations. Integrated spatial multi-omics analysis identified this layer as a primary site of molecular divergence in HC piglets, marked by coordinated up-regulation of genes from the turquoise and red co-expression modules. The turquoise module contained genes closely linked to synaptic vesicle biology and plasticity, including *CHGB* and *SNAP25*, which contribute to vesicle packaging and fusion, and *NRGN*, which supports calmodulin-dependent synaptic modulation. In parallel, reduced *CAMK2N1* expression suggested decreased inhibition of calcium signaling,

potentially facilitating calcium-mediated plasticity. The red module included *PVALB*, a calcium-buffering protein enriched in GABAergic interneurons, and *SCN1B*, a regulator of sodium channel kinetics and action potential timing. Together, these layer III signatures suggest a coordinated transcriptional program that may strengthen neural precision, temporal synchrony, and synaptic adaptability within a key associative cortical layer.

Single-cell transcriptomic analysis provided cellular context for interpreting these spatially organized molecular patterns. *PVALB* was confirmed as a marker of a specific GABAergic interneuron subtype. Notably, the absence of differential expression in canonical pan-GABAergic neuronal markers *GAD1* (*P*-adjust=1; $\log_2$FC=0.0532) and *GAD2* (*P*-adjust=1; $\log_2$FC=0.0273) between HC and LC groups indicated that *PVALB* up-regulation likely reflects enhanced functional specialization rather than an increased abundance of GABAergic neurons. This finding suggests that improved cognitive performance may be associated with a functional augmentation of specific inhibitory circuits, rather than broad expansion of the inhibitory neuronal population.

Single-cell analysis also revealed distinct cellular expression patterns for other cognition-associated candidates. Both *CHGB* and *CRYM* were predominantly expressed in excitatory neurons, whereas *SCN1B* showed preferential expression in inhibitory neurons. These specific cellular distributions indicate complementary roles within cortical circuitry: *CHGB* and *CRYM* likely modulate excitatory transmission and metabolic processes in glutamatergic neurons, whereas *SCN1B* may fine-tune inhibitory control mechanisms.

Integrated gene-metabolite networks fine-tune synaptic plasticity

The identified genes and associated metabolites formed an integrated regulatory network that links synaptic vesicle trafficking, calcium-dependent plasticity, metabolic control, and neuronal excitability. *SNAP25* and *CHGB* provide a molecular basis for regulated vesicle dynamics and neurotransmitter release. After synaptic activation, glutamatergic signaling may be calibrated through opposing influences of *NRGN*, which promotes calmodulin-dependent CaMKII signaling, and *CAMK2N1*, which constrains this pathway, thereby enabling precise control of synaptic strength. *CRYM* may further modulate neurotransmission through metabolic regulation of glutamate and GABA availability, supporting excitatory/inhibitory balance at the biochemical level. In parallel, *PVALB* contributes to intracellular calcium buffering, supported by glutathione-associated antioxidant capacity, whereas *SCN1B* regulates membrane excitability and action potential timing. This coordinated network may provide both stability and flexibility within cortical circuits, thereby supporting higher cognitive performance (Figure 4A).

Energetic and metabolic underpinnings of cognition

Enhanced synaptic activity imposes substantial energetic demands (Harris et al., 2012; Watts et al., 2018), and the spatial metabolomic profiles of HC piglets were consistent with adaptive metabolic remodeling. Altered pathways related to aerobic glycolysis and the pentose phosphate pathway suggest an adaptive metabolic state that balances ATP production with oxidative stress management (Figure 4B–F) (Bélanger et al., 2011; Cheng et al., 2022; Dienel, 2019; Magistretti & Allaman, 2015; Yellen, 2018). This interpretation was supported by increased abundance or expression of glycolytic components, including *ENO1*, TCA cycle-related intermediates, and glutathione metabolism components in HC piglets, indicating a shift towards a metabolic program capable of meeting high energy requirements while mitigating oxidative burden. This energetic underpinning, revealing a trade-off between energy production and oxidative stress, may be essential for sustaining the heightened neural computation and synaptic plasticity associated with superior cognitive performance (Butterfield & Halliwell, 2019; Dionísio et al., 2021; Zhao et al., 2019).

Advancing pig cognitive research and cross-species translational implications

This study extends beyond previous bulk and single-cell porcine omics analyses (Fang et al., 2012; Lin et al., 2000; Zhang et al., 2013; Zhu et al., 2021) by integrating spatial transcriptomic and metabolomic profiling to resolve layer-specific molecular networks in the prefrontal cortex. This spatial resolution was essential for identifying localized transcriptional and metabolic programs associated with cognitive variation within the laminated cortical architecture, challenging the notion that cognitive ability is governed solely by global expression changes. Cross-species validation further strengthened the translational relevance of these findings. Conserved up-regulation of *CHGB*, *PVALB*, *SCN1B*, and *CRYM* in HC mice suggests that these genes belong to an evolutionarily conserved module associated with cognitive performance. This conservation, coupled with the gyrencephalic architecture and human-relevant neuroanatomical organization of the pig brain (Ryan et al., 2018), supports the predictive value of the porcine model for translational neuroscience (Qiu et al., 2024; Todea et al., 2020). Notably, genes such as *CHGB*, which is involved in synaptic release (Mukherjee et al., 2025), and *NRGN*, which is involved in calcium signaling (Castrogiovanni et al., 2021; Li et al., 2024), have established roles in human neurocognitive disorders, including Alzheimer's disease and schizophrenia. These findings therefore provide a spatially resolved molecular framework for investigating cognitive enhancement and neuroprotective strategies.

Limitations and future directions

Although this study generated a high-resolution spatial molecular atlas of the porcine prefrontal cortex, several limitations remain. Additional layer-resolved validation using complementary approaches, such as laser capture microdissection followed by qPCR, would further strengthen the anatomical precision of the findings. Future work should incorporate functional perturbation studies, including CRISPR-based approaches, to establish causal links between candidate genes and cognitive phenotypes. Expanding this comparative framework to non-human primates and human postmortem brain tissue would further clarify the translational relevance of the identified molecular programs.

CONCLUSION

Integrated spatial transcriptomic and metabolomic profiling identified layer-enriched gene-metabolite networks associated with cognitive variation in pigs. Cross-species validation further highlighted *CHGB* as a conserved cognition-associated gene within this network. These findings define a spatially resolved molecular architecture for understanding cognitive function in a large gyrencephalic brain and provide a foundation for comparative analysis of laminated brain structures across species. The identified molecular signatures

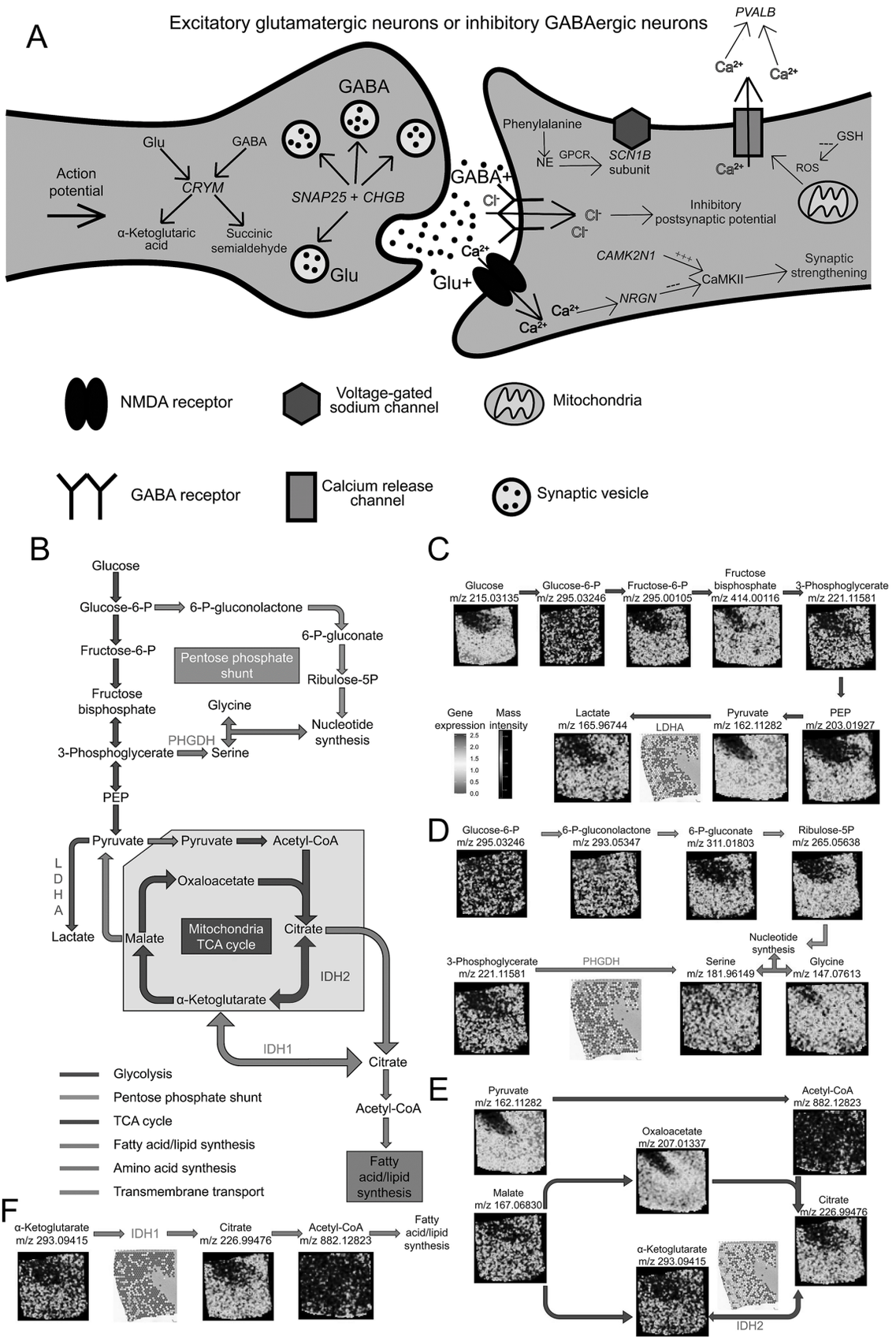

Figure 4 Simplified schematic of molecular mechanisms in synaptic transmission and aerobic glycolysis

A: Simplified schematic showing cognition-associated genes involved in synaptic activity. B–F: Spatial schematics showing genes and metabolites associated with aerobic glycolysis and related metabolic pathways. Note: This conceptual model integrates molecular mechanisms from excitatory (glutamatergic) and inhibitory (GABAergic) neurons to illustrate coordinated circuit-level regulation. *In vivo*, glutamate and GABA are typically packaged and released from distinct presynaptic terminals.

may inform future strategies aimed at enhancing cognitive resilience in agricultural and biomedical contexts.

DATA AVAILABILITY

The spatial transcriptomic data generated in this study were deposited in the NCBI database (accession number GSE272894), GSA database (accession number CRA038099), and Science Data Bank (https://doi.org/10.57760/sciencedb.j00139.00331). The spatial metabolomics data were deposited in the Metaspace database (https://metaspace2020.org/project/pig_brain). Video recordings of the cognitive tests are stored in the Zenodo database and can be accessed at https://doi.org/10.5281/zenodo.17174975. Public single-cell data were obtained from the CNGBdb (accession number CNP0000686).

SUPPLEMENTARY DATA

Supplementary data for this article can be found online.

COMPETING INTERESTS

The authors declare that they have no competing interests.

AUTHORS' CONTRIBUTIONS

G.Q.T., S.D.C., and J.G.W. conceived and designed the study. S.D.C., Z.J.Z., and Z.Y.C. conducted animal testing and data analysis. S.D.C., D.C., Q.S., Y.Y., J.M.C., and S.X.Y. collected brain samples. S.D.C. and D.C. performed spatial transcriptomics and metabolomics analysis. P.X.W., Z.Y.G., J.Y.W., and X.W.L. provided critical feedback and commented on the manuscript. G.Q.T. secured financial support for the research. S.D.C. and S.X.Y. drafted the manuscript. G.Q.T. supervised the research and edited the paper. All authors read and approved the final version of the manuscript.

ACKNOWLEDGMENTS

We thank Luming Biotech for providing spatial transcriptomics sequencing and AFADESI-MSI technology.

REFERENCES

Balaram P, Kaas JH. 2014. Towards a unified scheme of cortical lamination for primary visual cortex across primates: insights from NeuN and VGLUT2 immunoreactivity. *Frontiers in Neuroanatomy*, **8**: 81.

Bastos AM, Loonis R, Kornblith S, et al. 2018. Laminar recordings in frontal cortex suggest distinct layers for maintenance and control of working memory. *Proceedings of the National Academy of Sciences of the United States of America*, **115**(5): 1117–1122.

Baysoy A, Bai ZL, Satija R, et al. 2023. The technological landscape and applications of single-cell multi-omics. *Nature Reviews Molecular Cell Biology*, **24**(10): 695–713.

Bélanger M, Allaman I, Magistretti PJ. 2011. Brain energy metabolism: focus on astrocyte-neuron metabolic cooperation. *Cell Metabolism*, **14**(6): 724–738.

Bemis KA, Föll MC, Guo D, et al. 2023. Cardinal v. 3: a versatile open-source software for mass spectrometry imaging analysis. *Nature Methods*, **20**(12): 1883–1886.

Butterfield DA, Halliwell B. 2019. Oxidative stress, dysfunctional glucose metabolism and Alzheimer disease. *Nature Reviews Neuroscience*, **20**(3): 148–160.

Campbell JN, Macosko EZ, Fenselau H, et al. 2017. A molecular census of arcuate hypothalamus and median eminence cell types. *Nature Neuroscience*, **20**(3): 484–496.

Castrogiovanni P, Sanfilippo C, Imbesi R, et al. 2021. Brain *CHID1* expression correlates with *NRGN* and *CALB1* in healthy subjects and AD patients. *Cells*, **10**(4): 882.

Chen SF. 2023. Ultrafast one-pass FASTQ data preprocessing, quality control, and deduplication using fastp. *iMeta*, **2**(2): e107.

Chen SF, Zhou YQ, Chen YR, et al. 2018. fastp: an ultra-fast all-in-one FASTQ preprocessor. *Bioinformatics*, **34**(17): i884–i890.

Cheng XT, Huang N, Sheng ZH. 2022. Programming axonal mitochondrial maintenance and bioenergetics in neurodegeneration and regeneration. *Neuron*, **110**(12): 1899–1923.

Dai JX, Ma YB, Le NY, et al. 2018. Large animal models of traumatic brain injury. *International Journal of Neuroscience*, **128**(3): 243–254.

Dienel GA. 2019. Brain glucose metabolism: integration of energetics with function. *Physiological Reviews*, **99**(1): 949–1045.

Dionísio PA, Amaral JD, Rodrigues CMP. 2021. Oxidative stress and regulated cell death in Parkinson's disease. *Ageing Research Reviews*, **67**: 101263.

Fang XD, Mou YL, Huang ZY, et al. 2012. The sequence and analysis of a Chinese pig genome. *GigaScience*, **1**(1): 16.

Friess SH, Ichord RN, Owens K, et al. 2007. Neurobehavioral functional deficits following closed head injury in the neonatal pig. *Experimental Neurology*, **204**(1): 234–243.

Hao YH, Hao S, Andersen-Nissen E, et al. 2021. Integrated analysis of multimodal single-cell data. *Cell*, **184**(13): 3573–3587. e29.

Harris JJ, Jolivet R, Attwell D. 2012. Synaptic energy use and supply. *Neuron*, **75**(5): 762–777.

Howard JT, Ashwell MS, Baynes RE, et al. 2018. Genetic parameter estimates for metabolizing two common pharmaceuticals in swine. *Frontiers in Genetics*, **9**: 40.

Kinder HA, Baker EW, Howerth EW, et al. 2019. Controlled cortical impact leads to cognitive and motor function deficits that correspond to cellular pathology in a piglet traumatic brain injury model. *Journal of Neurotrauma*, **36**(19): 2810–2826.

Kornum BR, Knudsen GM. 2011. Cognitive testing of pigs (*Sus scrofa*) in translational biobehavioral research. *Neuroscience & Biobehavioral Reviews*, **35**(3): 437–451.

Lau SF, Cao H, Fu AKY, et al. 2020. Single-nucleus transcriptome analysis reveals dysregulation of angiogenic endothelial cells and neuroprotective glia in Alzheimer's disease. *Proceedings of the National Academy of Sciences of the United States of America*, **117**(41): 25800–25809.

Li MF, Shen TQ, Yao R, et al. 2024. Mitochondrial dysfunction is associated with cognitive impairment in adults with OSA without dementia. *Sleep Medicine*, **119**: 234–243.

Lin J, Barb CR, Matteri RL, et al. 2000. Long form leptin receptor mRNA expression in the brain, pituitary, and other tissues in the pig. *Domestic Animal Endocrinology*, **19**(1): 53–61.

Magistretti PJ, Allaman I. 2015. A cellular perspective on brain energy metabolism and functional imaging. *Neuron*, **86**(4): 883–901.

McGinnis CS, Murrow LM, Gartner ZJ. 2019. DoubletFinder: doublet detection in single-cell RNA sequencing data using artificial nearest neighbors. *Cell Systems*, **8**(4): 329–337. e4.

Mendl M, Laughlin K, Hitchcock D. 1997. Pigs in space: spatial memory and its susceptibility to interference. *Animal Behaviour*, **54**(6): 1491–1508.

Moffitt JR, Bambah-Mukku D, Eichhorn SW, et al. 2018. Molecular, spatial, and functional single-cell profiling of the hypothalamic preoptic region. *Science*, **362**(6416): eaau5324.

Morabito S, Reese F, Rahimzadeh N, et al. 2023. hdWGCNA identifies co-expression networks in high-dimensional transcriptomics data. *Cell Reports Methods*, **3**(6): 100498.

Mukherjee C, Chauksey P, Jain A, et al. 2025. Chromogranin B: a versatile neuroendocrine protein regulating physiological and metabolic functions. *Neuropeptides*, **113**: 102548.

Netzley AH, Pelled G. 2023. The pig as a translational animal model for biobehavioral and neurotrauma research. *Biomedicines*, **11**(8): 2165.

Poulin JF, Gaertner Z, Moreno-Ramos OA, et al. 2020. Classification of midbrain dopamine neurons using single-cell gene expression profiling approaches. *Trends in Neurosciences*, **43**(3): 155–169.

Qiu S, Jia JY, Xu BL, et al. 2024. Development and evaluation of an autism

pig model. *Lab Animal*, **53**(12): 376–386.
Qiu ZL, Li X. 2017. Non-human primate models for brain disorders - Towards genetic manipulations *via* innovative technology. *Neuroscience Bulletin*, **33**(2): 247–250.
Race AM, Styles IB, Bunch J. 2012. Inclusive sharing of mass spectrometry imaging data requires a converter for all. *Journal of Proteomics*, **75**(16): 5111–5112.
Ryan MC, Sherman P, Rowland LM, et al. 2018. Miniature pig model of human adolescent brain white matter development. *Journal of Neuroscience Methods*, **296**: 99–108.
Satija R, Farrell JA, Gennert D, et al. 2015. Spatial reconstruction of single-cell gene expression data. *Nature Biotechnology*, **33**(5): 495–502.
Silverman JL, Thurm A, Ethridge SB, et al. 2022. Reconsidering animal models used to study autism spectrum disorder: current state and optimizing future. *Genes, Brain and Behavior*, **21**(5): e12803.
Singh R, Kulikowicz E, Santos PT, et al. 2019. Spatial T-maze identifies cognitive deficits in piglets 1 month after hypoxia-ischemia in a model of hippocampal pyramidal neuron loss and interneuron attrition. *Behavioural Brain Research*, **369**: 111921.
Sorby-Adams AJ, Vink R, Turner RJ. 2018. Large animal models of stroke and traumatic brain injury as translational tools. *American Journal of Physiology-Regulatory, Integrative and Comparative Physiology*, **315**(2): R165-R190.
Swindle MM, Makin A, Herron AJ, et al. 2012. Swine as models in biomedical research and toxicology testing. *Veterinary Pathology*, **49**(2): 344–356.
Todea RA, Lu PJ, Fartaria MJ, et al. 2020. Evolution of cortical and white matter lesion load in early-stage multiple sclerosis: correlation with neuroaxonal damage and clinical changes. *Frontiers in Neurology*, **11**: 973.
Vandereyken K, Sifrim A, Thienpont B, et al. 2023. Methods and applications for single-cell and spatial multi-omics. *Nature Reviews Genetics*, **24**(8): 494–515.
Vink R. 2018. Large animal models of traumatic brain injury. *Journal of Neuroscience Research*, **96**(4): 527–535.
Watts ME, Pocock R, Claudianos C. 2018. Brain energy and oxygen metabolism: emerging role in normal function and disease. *Frontiers in Molecular Neuroscience*, **11**: 216.
Yellen G. 2018. Fueling thought: management of glycolysis and oxidative phosphorylation in neuronal metabolism. *Journal of Cell Biology*, **217**(7): 2235–2246.
Yu GC, Wang LG, Han YY, et al. 2012. clusterProfiler: an R package for comparing biological themes among gene clusters. *OMICS: A Journal of Integrative Biology*, **16**(5): 284–287.
Zhang LF, Cai ZW, Wei SJ, et al. 2013. MicroRNA expression profiling of the porcine developing hypothalamus and pituitary tissue. *International Journal of Molecular Sciences*, **14**(10): 20326–20339.
Zhao RZ, Jiang S, Zhang L, et al. 2019. Mitochondrial electron transport chain, ROS generation and uncoupling (Review). *International Journal of Molecular Medicine*, **44**(1): 3–15.
Zheng GXY, Terry JM, Belgrader P, et al. 2017. Massively parallel digital transcriptional profiling of single cells. *Nature Communications*, **8**: 14049.
Zhu JC, Chen F, Luo LH, et al. 2021. Single-cell atlas of domestic pig cerebral cortex and hypothalamus. *Science Bulletin*, **66**(14): 1448–1461.